Journal Name

ARTICLE

Amperometric magnetobiosensors using poly(dopamine)-modified Fe_3O_4 magnetic nanoparticles for the detection of phenolic compounds†

Received 00th January 20xx,
Accepted 00th January 20xx

DOI: 10.1039/x0xx00000x

www.rsc.org/

Miriam Martín[a], Pedro Salazar[a,b,*], Susana Campuzano[c], Reynaldo Villalonga[c], José Manuel Pingarrón[c], and José Luis González-Mora[a]

The synthesis of poly(dopamine)-modified magnetic nanoparticles (MNPs) and their application to prepare electrochemical enzyme biosensor useful to detect phenolic compounds is reported in this work. MNPs of about 16 nm were synthetized by co-precipitation method and conveniently modified with poly(dopamine). Non-modified and modified MNPs were characterized using X-ray photoelectron spectroscopy (XPS), Raman and infrared spectroscopy, X-ray diffraction (XRD) and atomic force microscopy (AFM). Horseradish peroxidase (HRP) was covalently immobilized onto the surface of the poly(dopamine)-modified MNPs via Michael addition and/or Schiff base formation and used to construct a biosensor for phenolic compounds by capturing the HRP-modified-nanoparticles onto the surface of a magnetic-modified glassy carbon electrode (GCE). Cyclic voltammetry and amperometry were used to study the electrochemical and analytical properties of the biosensor using hydroquinone (HQ) as redox probe. Among different phenolic compounds studied the biosensor exhibited higher sensitivity for HQ, 1.38 A M^{-1} cm^{-2}, with limits of detection and quantification of 0.3 and 1.86 µM, respectively. The analytical biosensor performance for HQ and 2-aminophenol compared advantageously with previous phenolic biosensors reported in the literature.

Introduction

The Electrode surface modification is a widely used electroanalytical strategy useful for many biosensing applications requiring highly biocompatible and properly functionalized surfaces to anchor the biorecognition material. In this context, conventional methods for enzyme immobilization are usually aggressive, long-time requiring and could be complicated or even not applicable to all surfaces [1-4]. Thus, easy, efficient and versatile immobilization methods are required in biosensor development [3].

Poly(dopamine) (pDA), a mussel-inspired coating, has recently attracted considerable attention for researchers. Early studies showed that the presence of 3,4-dihydroxy-L-phenylalanine (DOPA) and lysine-rich proteins were responsible for the extremely robust adhesion of mussels [3, 5-8]. In 2007, Lee et al. reported the first publication using dopamine (DA), with a similar molecular structure of DOPA, to obtain an adhesive pDA film [5, 7, 9]. Later on new pDA properties as well as interesting applications in biosensors, sensors, remediation, biomineralization, drug delivery and hyperthermia have been reported [3, 6-15]. The very reactive residual quinone groups in pDA allow further derivatizations with nitrogen and thiol residues through Schiff base formation or Michael-type addition respectively [3, 6, 7, 16, 17]. This high reactivity and the possibility to cover almost unlimited number of materials offer a great opportunity of further modifications [3, 6, 9]. In the particular case of biosensor development, pDA provides a suitable microenvironment for immobilizing a high density of biomolecules onto the transducer surface thus representing an easy, convenient and non-aggressive method to prepare biosensors. Furthermore, the biological material is firmly anchored by covalent bonding preserving its catalytic activity [16, 17].

Magnetic nanoparticles (MNPs) have gained a lot of attention in biomedical and industrial applications due to their biocompatibility, easy synthesis and ability of surface modification [18-23]. Moreover, they provide a large surface area for attachment of biorecognition elements and can then be easily separated from the liquid phase by a magnet, and spread immediately to zoom out which results highly appropriate in sensor and biosensor applications [16, 17, 22]. MNPs also provide a favorable microenvironment for electrochemical devices where enzymes may exchange electrons directly with

[a] Neurochemistry and Neuroimaging Group, (Laboratory of Sensors, Biosensors and Materials) Faculty of Medical Sciences, University of La Laguna, Campus de Ofra s/n, 38071 La Laguna, Tenerife (Spain).
[b] Laboratory of Nanotechnology on Surfaces, Institute of Materials Science of Seville (CSIC-Univ. Seville), Calle Américo Vespucio 49, 41092, Seville (Spain).
[c] Department of Analytical Chemistry, Faculty of Chemistry, Complutense University of Madrid, 28040, Madrid (Spain).

*psalazar@icmse.csic.es; psalazar@ull.edu.es

†Electronic Supplementary Information (ESI) available: See DOI: 10.1039/x0xx00000x

the transducer, improving the sensitivity and selectivity of electrochemical biosensors [24-29].

Phenolic compounds constitute a large group of organic pollutants which should be monitored in environmental engineering [30, 31]. Although, standard methods are adequate for quantitative phenolic determination [30, 32-35], generally they require pretreatment processes and high-qualified personnel. In addition, traditional electrochemical sensors are very poor and the electrode surface may be fouled by insulating polymer films or by-products generated during phenolic detection [36, 37]. Owing to those disadvantages, researchers have focused on the use on nanostructured and catalytic materials [31, 38, 39] or in enzyme based amperometric biosensors [40-47].

In the present work we combine the advantages raised by the use of Fe_3O_4 MNPs and pDA to develop an amperometric enzyme (HRP) biosensor for phenolic compounds. MNPs, synthesized by co-precipitation method, were coated with poly(dopamine) film forming a *core-shell* polymeric-Fe_3O_4 MNPs structure (Fe_3O_4@pDA MNPs) where HRP was immobilized. Although, HRP was immobilized using different approaches, few reports have been described in the literature using pDA as immobilization matrix [40-47]. The modified MNPs were characterized using different techniques such as XPS, AFM, FTIR, X-ray and the electroanalytical performance of the as prepared biosensor were evaluated against some common phenolic compounds.

Experimental

Reagents and solutions

HRP (type VI, EC 1.11.1.7, 269 U mg^{-1} solid), DA, HQ, H_2O_2 and all other chemicals were obtained from Sigma. Electrochemical experiments were performed in PBS buffer solution (10 mM sodium phosphate containing 2.7 mM KCl and 137 mM NaCl) of pH 7.4. DA solutions were prepared in PBS solution (pH 8.5) before using.

Instruments

All electrochemical measurements were performed with a DRP-STAT200 potentiostat and data were acquired with Dropview software (DropSens). An Ag/AgCl (3M KCl), a Pt wire and a home-made glassy carbon electrode (GCEs, 3 mm diameter) with magnetic electrical contact were used as reference, counter and working electrodes, respectively. Transmittance spectra (UV-Vis) of nanoparticles, pDA, HRP solutions were recorded in the range of 320-700 nm with respect to water using a Benchmark Plus microplate spectrophotometer (Bio-Rad). Raman spectra were recorded with a HORIBA HR-800-UV microscope. FT-IR spectra were recorded with respect to air, using a Varian 670-IR spectrophotometer in the range of 4000-400 cm^{-1}. The X-ray diffraction (XRD) pattern was recorded using a Philips Panalytical X'Pert powder diffractometer with Cu Kα (λ= 1.540 Å) radiation. The XPS spectra were collected on an ESCALAB 250 spectrometer, using a monochromatized Al Kα X-ray radiation (hv = 1486.6 eV). High resolution spectra were deconvoluted using the XPS peak 4.1 packet software. Images to characterize the size and distribution of non- and functionalized MNPs were performed by atomic force microscopy (AFM) using highly oriented pyrolytic graphite (HOPG) as substrate. Samples were imaged operating in tapping mode in air using a Multimode microscope and a Nanoscope V control unit from Bruker at a scan rate of 1.0-1.2 Hz. For this purpose, etched silicon tips (RTESP, 271-311 kHz, and 40-80 N m^{-1}) were used.

Preparation of Fe_3O_4@pDA/HRP MNPs

Fe_3O_4 magnetic nanoparticles were synthetized by co-precipitation method according to that reported earlier [16, 17]. Fe_3O_4@pDA *core-shell* nanoparticles were obtained by dispersing 500 mg of MNPs in 25 mL of 10 mM DA solution (PBS, pH 8.5) under continuous stirring during 4 hours. The resulting nanomaterial was then magnetically decanted and repeatedly washed with distilled water to remove the non-reacted monomer. To immobilize the enzyme, 50 mg of Fe_3O_4@pDA MNPs were dispersed in 2.5 mL of a 1 mg mL^{-1} HRP solution (PBS, pH 7.4) for 4 h under stirring at room temperature. The HRP-modified MNPs (Fe_3O_4@pDA/HRP MNPs) were magnetically decanted and washed thoroughly with PBS (pH 7.4) to remove the non-immobilized HRP, and further re-dispersed in PBS (pH 7.4) at 50 mg mL^{-1} final concentration and kept at 4 ºC.

Preparation of Fe_3O_4@pDA/HRP-GCE biosensor

For biosensor construction, GCEs were polished with 0.05 mm alumina slurry, rinsed thoroughly with water, then sonicated in water and acetone (3 minutes) and finally dried with N_2. Then, different volumes of Fe_3O_4@pDA/HRP MNPs suspension (at 2.5 mg mL^{-1} in PBS, pH 7.4) were transferred onto the surface of the GCE. This was done by keeping the GCE vertical and placing a neodymium magnet on the bottom part of the GC disk to localize in a reproducible way the Fe_3O_4@pDA/HRP MNPs onto the working surface, thus avoiding variations in the bead layer thickness or spreading area between different measurements. Before using we waited 1 min. for the full consolidation of the magnetic nanoparticles layer.

Electrochemical measurements

A conventional three-electrode system was used for cyclic voltammetry (CV) and constant potential amperometry (CPA) measurements using the biosensor as the working electrode. CV and CPA experiments were carried out in 15 mL PBS (pH 7.4) containing 2 mM H_2O_2 as enzyme substrate under constant magnetic stirring (700 rpm).

Results and discussion

Modified and unmodified magnetic nanoparticles were synthesized by coprecipitation of Fe^{2+}/Fe^{3+} ions in alkali media

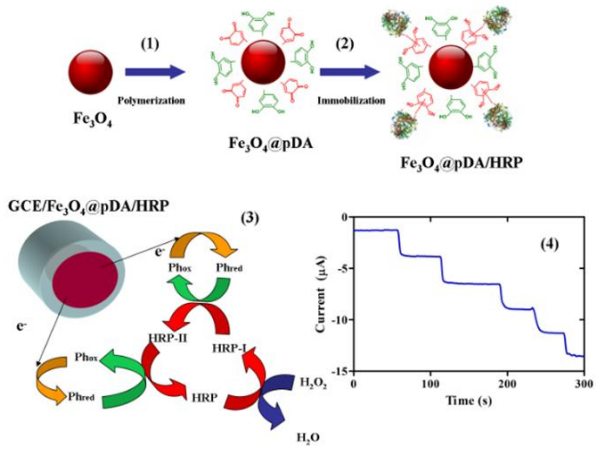

Scheme 1. Schematic illustration of the preparation of core–shell Fe_3O_4@pDA/HRP nanoparticles (1 and 2) and the Fe_3O_4@pDA/HRP-GCE biosensor (3) as well as the amperometric responses obtained for successive additions of 125 μL of 3 mM HQ (4).

and fully characterised by X-ray, XPS, AFM, UV-Vis, FT-IR and electrochemical techniques. **Scheme 1** displays the protocol used to prepare the functionalized Fe_3O_4@pDA/HRP MNPs and the Fe_3O_4@pDA/HRP-GCE biosensor.

Characterization of Fe_3O_4@pDA MNPs

XRD spectrum of synthesized Fe_3O_4 nanoparticle was in good agreement with magnetite pattern (Fe_3O_4; JCPDS card 75-0449) (**Figure S1** in *Supporting Information*). Crystallite size, calculated using the Debye-Scherrer, presented a value of ca. 16 nm.

AFM images for Fe_3O_4 MNPs and Fe_3O_4@pDA MNPs (**Figure 1)** show the formation of granular deposits formed by aggregated nanoparticles that partially cover the substrate surface. Non-modified nanoparticles (Fe_3O_4 MNPs) tended to adsorb mainly at HOPG steps meanwhile modified nanoparticles (Fe_3O_4@pDA MNPs) spread out to the HOPG terraces and aggregated giving rise to ramified islands. This finding may be justified taking into account the high reactivity of the different groups present on the polymer surface (mainly catechol and quinone moieties) and the strong π-π interactions between the basal plane of graphite and the aromatic subunits existing in the external polymeric shell. The size distribution for Fe_3O_4 MNPs (**Figure 1B** and **Table S1)** gives an average value of 15.29 nm with a narrow variability (SD=2.31). This value is in good agreement with that obtained by XRD analysis. Moreover, Fe_3O_4@pDA MNPs, **Figure 1D,** showed a larger diameter of 17.39 nm (SD=2.58) (**Table S1**), which is attributable to the pDA film thickness, ca. 2 nm.

XPS was used to confirm the nature of the MNPs and their successful core-shell structure. **Figure 2A** shows the raw spectrum for Fe_3O_4@pDA MNPs. The position of two Fe 2p peaks close to 720 eV and the O 1s peak at 284.6 eV confirmed the nature of the synthetized nanoparticles [48]. In addition, the high-resolution spectrum (**Figure 2B**) displayed the characteristic doublet, due to Fe $2p_{3/2}$ and Fe $2p_{1/2}$ core-level

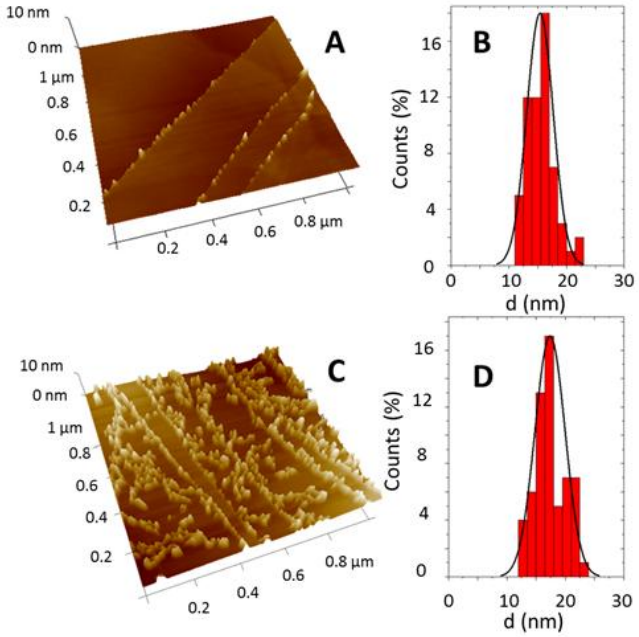

Figure 1. Typical 1x1 μm2 AFM images (A, C) and histograms showing particle-size distribution (B, D) for Fe_3O_4 (A, B) and Fe_3O_4@PDA MNPs (C, D).

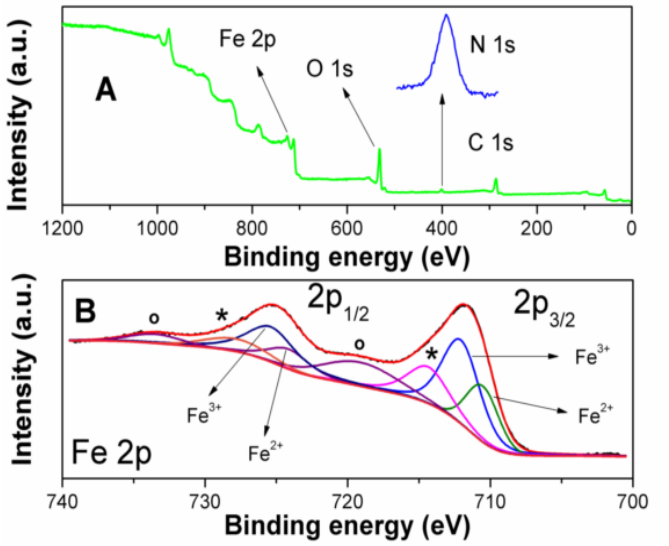

Figure 2. A) XPS spectra of e_3O_4@PDA MNPs; inset: expanded spectrum of the N1s core line. B) Deconvoluted high-resolution XPS spectra for Fe $2p_{3/2}$ and Fe $2p_{1/2}$ core-level lines for Fe_3O_4@PDA MNPs; (o) Fe^{3+} shake-up satellites and (*) Fe^{2+} shake-up satellites.

spectra of iron oxides at 710.9 and 724.5 eV respectively. The deconvolution of the two peaks in Fe^{2+} and Fe^{3+} oxidation states and their corresponding shake-up satellite contributions confirmed the presence of the magnetite phase. Finally, the presence of C 1s and N 1s peaks confirmed the core-shell configuration and the presence of pDA on the Fe_3O_4 MNPs surface (**Figure 2A**).

On the other hand, the intense Fe_3O_4 band (A1g mode) at 683 cm^{-1} in the Raman spectrum (**Figure 3)** confirms the magnetite phase in the Fe_3O_4@PDA MNPs. Other less intense phonon

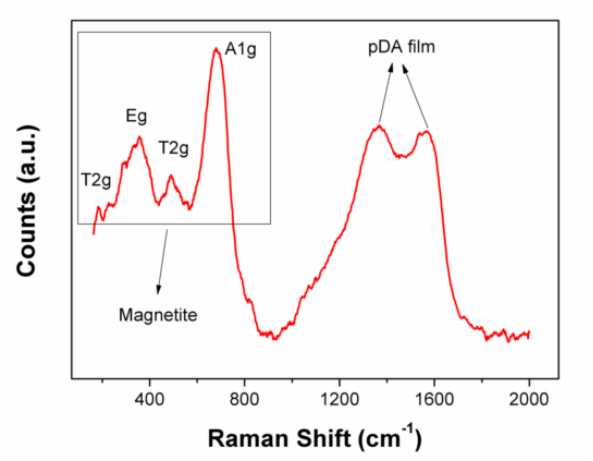

Figure 3. Raman spectrum of Fe_3O_4@PDA MNPs.

frequencies for Fe_3O_4 at 194 (T2g), 303 (Eg) and 528 (T2g) cm^{-1} were also identified [49]. Furthermore, Fe_3O_4@PDA MNPs presented two overlapping peaks at ca. 1,400 cm^{-1} associated to the stretching of catechol and 1,600 cm^{-1} associated to the deformation of catechol, thus confirming the core-shell configuration [50].

Characterization of Fe_3O_4@pDA/HRP MNPs

FT-IR spectroscopy was employed to monitor each Fe_3O_4 MNPs modification step. **Figure 4A** gathers the corresponding spectrum for each individual component (HRP, DA, pDA and MNPs) and also for the final modified adduct (Fe_3O_4@pDA/HRP MNPs). The FT-IR spectrum for free HRP exhibited the well characterized HRP amide I and II bands at 1,656 and 1,546 cm^{-1} [51] corresponding to C=O stretching vibration of peptide linkages and N-H bending and C-N stretching vibration in the protein backbone. DA showed relatively broad and strong bands in the 3,000-3,400 cm^{-1} region, assigned to the aromatic O-H asymmetry stretching vibration of CH_2 groups. Other relevant peaks appeared at 1,602 cm^{-1} due to overlap of C=C resonance vibrations in aromatic ring and 1,519 cm^{-1} (N-H scissoring vibrations) [52, 53]. Moreover, the spectrum for pDA displayed a large relative absorbance in the 1,500-1,100 cm^{-1} region, due to the polymer formation, attributable to C-O and C-N functional groups [16, 17]. FT-IR spectra of Fe_3O_4 MNPs nanoparticles (Fig. 4A) showed a main adsorption band around 580 cm^{-1}, corresponding to the Fe-O stretching modes of magnetite [16, 17], whereas Fe_3O_4@pDA/HRP MNPs showed an additional band, in the range of 1,000-1,700 cm^{-1}, with respect to non-modified Fe_3O_4 MNPs which may be ascribed to: (1) the aromatic rings of pDA, (2) the C-N stretching in the new Schiff bases formed during pDA polymerization and enzyme immobilization. Accordingly, the FT-IR results corroborated the successful attachment of HRP to the pDA-modified MNPs surface.

The HRP loading onto the polymeric surface was evaluated at different immobilization times using the characteristic UV-Vis

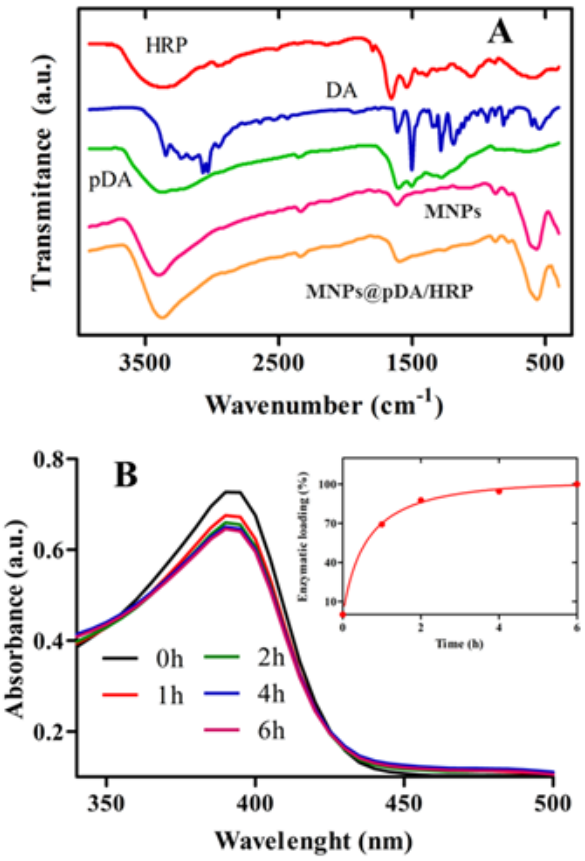

Figure 4. (A) FTIR transmittance spectra of HRP, DA, pDA, Fe_3O_4 MNPs, and Fe_3O_4@pDA/HRP MNPs. (B) Absorbance spectra for HRP solutions before (0 h) and after enzyme immobilization (1, 2, 4, 6 h); Inset: enzymatic loading obtained from absorbance data assuming the steady-state is reached after 6 hours.

band of HRP at 420 nm. The amount of immobilized HRP on the nanoparticles surface was calculated as the difference between the initial and final concentration in the enzyme solution upon the immobilization step was accomplished. Visible spectra for different times are displayed in Figure 4B showing an absorbance maximum decrease with the incubation time. Almost 70% of the HRP was attached onto the Fe_3O_4@PDA MNPs during the first hour (inset), and a levelling off was observed after 6 hours. Accordingly, the amount of immobilized HRP was estimated to be ca. 22 μg mg^{-1} for 6 h.

Electrochemical characterization of Fe_3O_4@pDA/HRP MNPs

GCE/Fe_3O_4@pDA/HRP biosensor was constructed by transferring the HRP-modified nanoparticles onto the surface of the GCE. Using a neodymium magnet located at the bottom part of the GC disk, Fe_3O_4@pDA/HRP MNPs were magnetically captured in a reproducible way. The electrochemical detection of phenolic compounds was achieved thanks to the ability of such compounds to re-oxidized the HRP enzyme, acting as electron shuttles from the redox centre of the HRP molecules to the GCE surface in the presence of H_2O_2 following the *double displacement* or "*ping-pong*" mechanism [40-47].

HQ was employed as a model compound in order to optimize the biosensor response against such substrates. **Figure 5A** shows cyclic voltammograms recorded for different HQ concentrations ranging from 0 to 0.9 mM. Both the anodic and cathodic peak currents increased linearly with the HQ concentration (inset in Fig. 5A). Moreover, the dependence of the peak currents for 1 mM HQ with the scan rate (v) was also checked (Fig. 5B). Both the anodic and cathodic peak currents exhibited a linear dependence with $v^{1/2}$, indicating a semi-infinite linear diffusion-controlled process [54-56]:

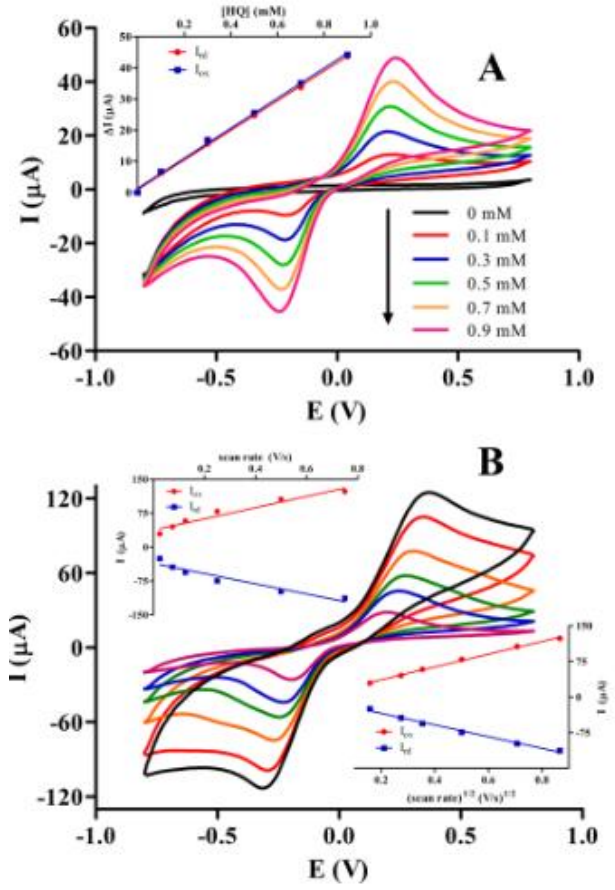

Figure 5. (A) CVs recorded at a GCE/Fe_3O_4@pDA/HRP biosensor in PBS solution, pH 7.4 containing different HQ concentrations (scan rate: 100 mV s^{-1}); inset: linear dependence between HQ concentration and the anodic (I_{ox}) and cathodic (I_{rd}) peak current values. (B) CVs recorded at a GCE/Fe_3O_4@pDA/HRP biosensor in PBS containing 1 mM HQ at different scan rates; insets: dependence of the anodic and cathodic peak current values with the scan rate and the square-root of the scan rate.

Constant potential amperometry (CPA) was used to test the electroanalytical performance of the Fe_3O_4@pDA/HRP MNPs. The detection potential was fixed to –0.2 V according to previous publications [16]. **Figure S2** shows the biosensor response against HQ before and after adding H_2O_2. As expected, only in presence of H_2O_2 the biosensor displayed a significant response, almost 2 orders of magnitude higher than in its absence. Experimental parameters such as the H_2O_2 concentration and the amount of Fe_3O_4@pDA/HRP MNPs magnetically captured onto the GCE surface were optimized

Table 1. Comparison of the analytical characteristics for different phenolic compounds using amperometric detection (E_{app} = –0.2 V, with 2 mM H_2O_2) at GCE/ Fe_3O_4@pDA/HRP.

Compounds	Sensitivity mean ± SD (A M^{-1} cm^{-2})	LOD (μM)	LQ (μM)	r^2
HQ	1.38±0.12	0.30	0.93	0.999
2-aminophenol	0.38±0.05	1.11	3.44	0.993
4-aminophenol	0.43±0.03	1.00	3.10	0.992

the results being described in *Supporting Information*. The amperometric signal increased with the amount of Fe_3O_4@pDA/HRP MNPs until 70 μg and then the signal decreased (**Figure S3A**) which was attributed to the increase in the electron transfer resistance for large Fe_3O_4@pDA/HRP MNPs loadings. Regarding H_2O_2 concentration (**Figure S3B)**, 2 mM was enough to ensure that the substrate concentration was not the limiting factor in the enzymatic reaction.

Figure 6 shows the amperometric responses of the GCE/Fe_3O_4@pDA/HRP biosensor for successive HQ additions with a response time ca. 7 s. (see **Figure S4)**. As it can be seen in **Figure S5**, the current response of the biosensor exhibited a linear dependence until 100 μM HQ with a high sensitivity of 1.38 A M^{-1} cm^{-2} (R^2 = 0.999). The calculated limits of detection (LOD) (at signal/noise = 3) and quantification (LQ) (at signal/noise = 10) were 0.3 and 0.93 μM, respectively.

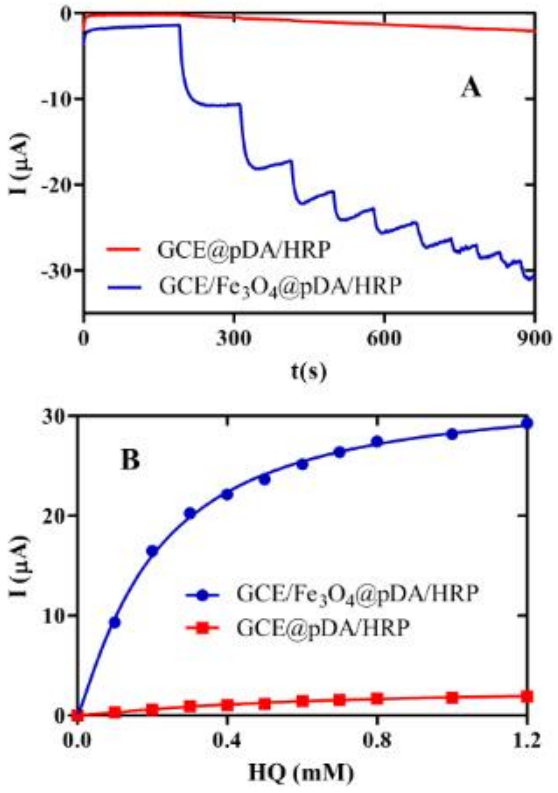

Figure 6. Amperometric responses (A) and calibration curves (B) obtained for HQ at GCE@pDA/HRP and GCE/Fe_3O_4@pDA/HRP electrodes in PBS (pH 7.4) containing 2 mM H_2O_2 (E_{app} = -0.2 V vs Ag/AgCl).

This amperometric performance was compared with that observed for a non-nanostructured biosensor prepared by modifying a GCE with pDA and HRP (GCE@pDA/HRP electrode)

using the same construction protocol to that employed for the nanoparticles-modified biosensor (**Figure 6)**. The achieved sensitivity for HQ, ca. 0.04 A M^{-1} cm^{-2}, was much smaller than that attained with the biosensor prepared with Fe_3O_4@pDA/HRP MNPs. A comparison of the enzyme kinetics parameters using the Hill modified Michaelis-Menten equations yielded values of K_M = 157 µM; V_{max} = 32.71 µA and Hill parameter (h) = 1.2 for the GCE/Fe_3O_4@pDA/HRP biosensor, while they were K_M = 461 µM; V_{max} = 2.65 µA and h = 1.2 for the GCE@pDA/HRP biosensor. The much better performance found for the MNPs-modified electrodes can be attributed to the synergism between the large nanoparticles surface and the efficient enzyme immobilization onto the polymer surface.

The analytical characteristics of the calibration plots recorded for HQ and other polyphenols over the 0 to 100 µM concentration range are shown and compared in **Table 1**. As it can be seen, the GCE/Fe_3O_4@pDA/HRP biosensor exhibited higher sensitivity and lower LOD and LQ for HQ. Also, no significant responses were obtained for phenol, m- and p-cresol. The trend in sensitivity is consistent with the ability of the electron-donor conjugation of the substituent and the ability to radical stabilization and to form resonance structures and the charge dissipation through the conjugated system [57-59]. Therefore, the absence of reactive groups in phenol and the presence of m- and p- methyl groups in the cresol molecule do not allow the formation of the conjugated structures**.**

The reproducibility and repeatability of the GCE/Fe_3O_4@pDA/HRP biosensor was evaluated by measuring the slope value of calibration plots for HQ in the 0-100 µM concentration range. Relative standard deviation (RSD) values were 3.8 and 6.5% for five calibrations plots constructed successively with the same electrode or with five different biosensors prepared in the same manner, respectively. These values demonstrated the feasibility of the biosensor fabrication procedure (which included the preparation of the Fe_3O_4@pDA/HRP MNPs and their magnetic capture onto the GCE surface) and the signal transduction methodology used. Finally, the stability of the Fe_3O_4@pDA/HRP MNPs was evaluated after storing them in PBS (pH 7.4) at 4 ºC for a time period of 1 month. No significant loss of the amperometric response obtained for 1 mM HQ with the biosensor constructed with the stored nanomaterial was observed (results not shown).

Comparison with other electrochemical HRP-based biosensor

Table 2 compares the analytical characteristics of the prepared biosensor with those reported for other electrochemical HRP-based biosensors for HQ and 2-AP determination. Such biosensors have been developed using different immobilization techniques and nanomaterials to improve the biosensor response. As it can be seen, the Fe_3O_4@pDA/HRP MNPs biosensor exhibits the best sensitivity and the lowest LOD for HQ. Although the analytical characteristics obtained for 2-AP are moderate, the approach described in this work results more convenient and easier when compared to more sensitive approaches.

Table 2. Electrochemical biosensors using HRP reported for HQ and 2-AP determination.

Configuration	Compound	Sensitivity	LOD (µM)	Linear range (µM)	Reference
GCE/MNPs@pDA/HRP	HQ	1.38 A M^{-1} cm^{-2}	0.3	0.30–150	this work
AuE/(ConA/HRP)n		0.61 A M^{-1} cm^{-2}	2.0	6–70	[46]
HRP/Met/MWCNT/GE		ca. 0.04 A M^{-1} cm^{-2}	-----	-----	[47]
GCE/PVF/PPy-HRP		15.32 nA μM^{-1}	0.6	1.6–15	[45]
GCE/CNT/PPy/HRP		0.11 A M^{-1} cm^{-2}	6.4	16–240	[41]
GCE/Poly(GMA-co-MTM)/PPy/CNT/HRP		0.13 A M^{-1} cm^{-2}	0.3	1.6-25.6	[41]
HRP-SiSG/AgNPs/poly(l-Arg)/CPE		-----	0.6	1–150	[44]
HRP-SiSG/CPE		-----	1.5	5–1000	[43]
GCE/MNPs@pDA/HRP	2-AP	0.38 A M^{-1} cm^{-2}	1.1	1.11–120	this work
AuE/(ConA/HRP)n		0.59 A M^{-1} cm^{-2}	0.5	3.7–25.9	[46]
AuE/Cys/Fe_3O_4–SiPGMA/HRP		0.004 A M^{-1} cm^{-2}	25	500-3500	[42]
GCE/PVF/PPy-HRP		15.25 nA μM^{-1}	0.7	1–20	[45]
GCE/CNT/PPy/HRP		0.57 A M^{-1} cm^{-2}	1.5	8–60.8	[41]
GCE/Poly(GMA-MTM)/PPy/CNT/HRP		0.03 A M^{-1} cm^{-2}	0.3	1.6–44.8	[41]

AgNPs: silver nanoparticles; AuE:Gold Electrode; CHIT: Chitosan; CNT: Carbon nanotube; ConA: Concavalin A; CPE: Carbon Paste Electrode; Cys: cysteine; GCE: Glassy Carbon Electrode; GE: Graphite Electrode; HRP: Horseradish peroxidase; Met: Methylene Blue; MNPs: magnetic nanoparticles; MWCNT:Multi-Wall Carbon Nanotubes; pDA: poly(dopamanine); Poly(l-Arg): poly(l-arginine); Poly(GMA-co-MTM): Poly(glycidyl methacrylate-co-3-thienylmethyl methacrylate); PPy: Polypirrole; PVF: Polyvinylferrocene; SiPGMA: silane polyglycidyl metacrylate; SiSG: silica sol–gel.

Conclusions

This paper describes the synthesis and application of HRP-modified magnetic nanoparticles to detect phenolic compounds. Enzyme has been successfully immobilized using a bioinspired polymer, poly(dopamine) and used to modify a GCE. The amount of the immobilized HRP was estimated to be ca. 22 µg mg-1. The electroanalytical properties of the reported biosensor confirmed the benefits of using nanostructured biosensors achieving a low KM value and comparing advantageously with previous HQ and 2-AP HRP-based biosensing strategies reported in the literature.

Acknowledgements

The financial support of the Spanish Ministerio de Economía y Competitividad Research Projects CTQ2011-24355, CTQ2012-34238, RECUPERA 2020 together with the "Fondo social Europeo", MAT2013-40852-R and MAT2013-42900-P and the Junta de Andalucía (TEP 8067 and FQM 6900) are gratefully acknowledged. Financial support from the NANOAVANSENS Program from the Comunidad de Madrid (S2013/MT-3029) is also gratefully acknowledged. R. Villalonga acknowledges a Ramón & Cajal contract from the Spanish Ministry of Science and Innovation.

References

1. S. Srivastava and N. A. Kotov, *Acc. Chem. Res.*, 2008, **41**, 1831-1841.
2. T. Gong, B. J. Adzima, N. H. Baker and C. N. Bowman, *Adv. Mater.*, 2013, **25**, 2024-2028.
3. Y. Liu, K. Ai and L. Lu, *Chem. Revi.*, 2014, **114**, 5057-5115.
4. J. Wang, D. F. Thomas and A. Chen, *Anal. Chem.*, 2008, **80**, 997-1004.
5. H. Lee, S. M. Dellatore, W. M. Miller and P. B. Messersmith, *Science*, 2007, **318**, 426-430.
6. E. Faure, C. Falentin-Daudré, C. Jérôme, J. Lyskawa, D. Fournier, P. Woisel and C. Detrembleur, *Prog. Polym. Sci.*, 2013, **38**, 236-270.
7. D. R. Dreyer, D. J. Miller, B. D. Freeman, D. R. Paul and C. W. Bielawski, *Chem. Sci.*, 2013, **4**, 3796-3802.
8. D. R. Dreyer, D. J. Miller, B. D. Freeman, D. R. Paul and C. W. Bielawski, *Langmuir*, 2012, **28**, 6428-6435.
9. H. Lee, J. Rho and P. B. Messersmith, *Adv. Mat.*, 2009, **21**, 431-434.
10. W.-H. Zhou, C.-H. Lu, X.-C. Guo, F.-R. Chen, H.-H. Yang and X.-R. Wang, *J. Mat Chem*, 2010, **20**, 880-883.
11. M. E. Lynge, R. van der Westen, A. Postma and B. Stadler, *Nanoscale*, 2011, **3**, 4916-4928.
12. R. Luo, L. Tang, J. Wang, Y. Zhao, Q. Tu, Y. Weng, R. Shen and N. Huang, *Colloids Surf., B*, 2013, **106**, 66-73.
13. G. Loget, J. B. Wood, K. Cho, A. R. Halpern and R. M. Corn, *Anal. Chem.*, 2013, **85**, 9991-9995.
14. G. Wang, H. Huang, G. Zhang, X. Zhang, B. Fang and L. Wang, *Langmuir*, 2010, **27**, 1224-1231.
15. Y. Wan, D. Zhang, Y. Wang, P. Qi and B. Hou, *Biosens. Bioelectron.*, 2011, **26**, 2595-2600.
16. M. Martin, P. Salazar, R. Villalonga, S. Campuzano, J. M. Pingarron and J. L. Gonzalez-Mora, *J. Mater. Chem. B*, 2014, **2**, 739-746.
17. M. Martín, A. González Orive, P. Lorenzo-Luis, A. Hernández Creus, J. L. González-Mora and P. Salazar, *ChemPhysChem*, 2014, **15**, 3742-3752.
18. W. Wang, Y. Jing, S. He, J.-P. Wang and J.-P. Zhai, *Colloids Surf., B*, 2014, **117**, 449-456.
19. A. Cervadoro, M. Cho, J. Key, C. Cooper, C. Stigliano, S. Aryal, A. Brazdeikis, J. F. Leary and P. Decuzzi, *ACS Appl. Mater. Inter.*, 2014, **6**, 12939-12946.
20. Y. p. Chen, M. q. Zou, D. n. Wang, Y. l. Li, Q. Xue, M. x. Xie and C. Qi, *Biosens. Bioelectron.*, 2013, **43**, 6-11.
21. R. Sharma, Y. Xu, S. W. Kim, M. J. Schueller, D. Alexoff, S. D. Smith, W. Wang and D. Schlyer, *Nanoscale*, 2013, **5**, 7476-7483.
22. J. B. Haun, T.-J. Yoon, H. Lee and R. Weissleder, *WIREs Nanomed Nanobiotech*, 2010, **2**, 291-304.
23. C. Rümenapp, B. Gleich, H. G. Mannherz and A. Haase, *J. Magn. Magn. Mater.*, 2015, **380**, 271-275.
24. J. Jordan, C. S. S. R. Kumar and C. Theegala, *J. Mol. Catal. B: Enzym.*, 2011, **68**, 139-146.
25. W. Xie and N. Ma, *Biomass Bioenergy*, 2010, **34**, 890-896.
26. I. Willner, B. Willner and E. Katz, *Bioelectrochem.*, 2007, **70**, 2-11.
27. B. Esteban-Fernández de Ávila, V. Escamilla-Gómez, S. Campuzano, M. Pedrero and J. M. Pingarrón, *Electroanalysis*, 2013, **25**, 51-58.
28. B. Esteban-Fernández de Ávila, M. Pedrero, S. Campuzano, V. Escamilla-Gómez and J. Pingarrón, *Anal Bioanal. Chem.*, 2012, **403**, 917-925.
29. F. Conzuelo, M. Gamella, S. Campuzano, A. J. Reviejo and J. M. Pingarrón, *Anal. Chim. Acta*, 2012, **737**, 29-36.
30. T. Xie, Q. Liu, Y. Shi and Q. Liu, *J. Chromatogr. A*, 2006, **1109**, 317-321.
31. M. Buleandra, A. A. Rabinca, C. Mihailciuc, A. Balan, C. Nichita, I. Stamatin and A. A. Ciucu, *Sens. Actuators, B*, 2014, **203**, 824-832.
32. T. Hyötyläinen and K. Hartonen, *TrAC, Trends Anal. Chem*, 2002, **21**, 13-30.
33. Q. S. Usmani, M. M. Beg and I. C. Shukla, *Analyst*, 1979, **104**, 148-151.
34. C.-H. Lin, J.-Y. Sheu, H.-L. Wu and Y.-L. Huang, *J. Pharm. Biomed. Anal.*, 2005, **38**, 414-419.
35. T. J. Boyd, *J. Chromatogr. A*, 1994, **662**, 281-292.
36. W. Huang, D. Zhou, X. Liu and X. Zheng, *Environ. Technol.*, 2009, **30**, 701-706.
37. S. Lupu, C. Lete, M. Marin, N. Totir and P. C. Balaure, *Electrochim. Acta*, 2009, **54**, 1932-1938.
38. H. Dejmkova, M. Scampicchio, J. Zima, J. Barek and S. Mannino, *Electroanalysis*, 2009, **21**, 1014-1018.
39. S. Zhu, W. Niu, H. Li, S. Han and G. Xu, *Talanta*, 2009, **79**, 1441-1445.
40. X. Liu, L. Luo, Y. Ding and Y. Xu, *Analyst*, 2011, **136**, 696-701.
41. E. E. a. F. Y. Seyda Korkut Ozoner,in: Environmental Biosensors, Prof. Vernon Somerset (Ed.), ISBN: 978-953-307-486-3, InTech, 2011, DOI: 10.5772/16998.
42. E. Çevik, M. Şenel, A. Baykal and M. F. Abasıyanık, *Sens. Actuators, B*, 2012, **173**, 396-405.
43. K. Reddaiah, T. Madhusudana Reddy, P. Raghu and P. Gopal, *Anal. Bioanaly Electrochem*, 2012, **4**, 372-385.

44. P. Raghu, T. Madhusudana Reddy, K. Reddaiah, L. R. Jaidev and G. Narasimha, *Enzyme Microb. Technol.*, 2013, **52**, 377-385.
45. M. Topcu Sulak, E. Erhan and B. Keskinler, *Appl. Biochem. Biotechnol.*, 2010, **160**, 856-867.
46. S. Yang, Z. Chen, X. Jin and X. Lin, *Electrochim. Acta*, 2006, **52**, 200-205.
47. A. Santos, A. Pereira, M. Sotomayor, C. Tarley, N. Durán and L. Kubota, *Electroanalysis*, 2007, **19**, 549-554.
48. L. Zhuo, Y. Wu, L. Wang, J. Ming, Y. Yu, X. Zhang and F. Zhao, *J. Mater. Chem. A*, 2013, **1**, 3954-3960.
49. I. Chourpa, L. Douziech-Eyrolles, L. Ngaboni-Okassa, J.-F. Fouquenet, S. Cohen-Jonathan, M. Souce, H. Marchais and P. Dubois, *Analyst*, 2005, **130**, 1395-1403.
50. J. Ryu, S. H. Ku, H. Lee and C. B. Park, *Adv. Funct. Mater.*, 2010, **20**, 2132-2139.
51. L. Luo, L. Zhu, Y. Xu, L. Shen, X. Wang, Y. Ding, Q. Li and D. Deng, *Microchim. Acta*, 2011, **174**, 55-61.
52. B. Fei, B. Qian, Z. Yang, R. Wang, W. C. Liu, C. L. Mak and J. H. Xin, *Carbon*, 2008, **46**, 1795-1797.
53. Y. Ma, H. Niu, X. Zhang and Y. Cai, *Analyst*, 2011, **136**, 4192-4196.
54. P. Salazar, M. Martín, R. D. O'Neill, R. Roche and J. L. González-Mora, *Colloids Surf., B*, 2012, **92**, 180-189.
55. Y. She, Y. Tang, H. Liu and P. He, *Chem. Cent. J.*, 2010, **4**, 17-17.
56. X. Ji, C. E. Banks, D. S. Silvester, A. J. Wain and R. G. Compton, *J. Phys. Chem. C*, 2007, **111**, 1496-1504.
57. S. Yang, Y. Li, X. Jiang, Z. Chen and X. Lin, *Sens. Actuators, B*, 2006, **114**, 774-780.
58. S. S. Rosatto, P. T. Sotomayor, L. T. Kubota and Y. Gushikem, *Electrochim. Acta*, 2002, **47**, 4451-4458.
59. S. A. Kane, E. I. Iwuoha and M. R. Smyth, *Analyst*, 1998, **123**, 2001-2006.